Laser-Activated Gene Silencing *via* Gold Nanoshell−siRNA Conjugates

Gary B. Braun,[†] Alessia Pallaoro,[†] Guohui Wu,[‡] Dimitris Missirlis,[‡] Joseph A. Zasadzinski,[‡] Matthew Tirrell,[‡] and Norbert O. Reich[†,*]

[†]Department of Chemistry and Biochemistry and [‡]Department of Chemical Engineering and Materials Research Laboratory, University of California, Santa Barbara, California 93106

Spatially and temporally controlled delivery of molecules into living cells to perturb and interrogate cellular function is a technical challenge that is seemingly destined to be solved by nanoparticles (NPs). In principle, gold-based NPs can be simultaneously decorated with moieties to enhance stability, direct cell-specific targeting, subcellular localization, and release multiple "cargos" such as drugs. Nucleic acids are an actively pursued and biomedically relevant NP cargo which can elicit post-transcriptional regulation through either antisense DNA or RNA interference (RNAi) mechanisms. Currently available reagents such as Lipofectamine (Invitrogen), polyethyleneimine, and poly-L-lysine enhance cellular uptake of nucleic acids under *in vitro* conditions, challenging the development of NP-based strategies to provide new capabilities or other improvements. Tissue-specific *in vivo* delivery of nucleic acids and other agents using multifunctional NPs presents additional challenges. Recent gold NP-antisense[1] and small interfering RNA (siRNA) conjugates[2] demonstrate the *in vitro* functionality of these hybrid materials. Yet, high potency RNAi has not yet been achieved through optical activation of gold nanocarriers.

Highly relevant goals of designed cellular delivery include temporal and spatial control and targeting specific cell types and subcellular organelles.[3] Photocaging of nucleic acids, followed by UV release, has been used for light-controlled antisense delivery into cells.[4,5] However, the lack of available caging groups responsive at the more biologically friendly near-infrared (NIR) wavelength has generated interest in other methods of activation.[1,6] NIR release from a compactly integrated NP, which can carry many hundreds or thousands of cargo mol-

ecules, should form a versatile, trackable delivery vehicle for high-resolution drug release. Aspects of these goals have been achieved, most notably the use of laser-induced release of nucleic acids linked to gold-based nanorods.[1,6,7] Desorption of thiols from gold NPs (Au NPs) has generated particular interest as an optical handle for nucleic acid release into the surrounding fluid, due to the absorbance characteristics of gold, moderate thiol−Au bond strength, and synthetic ease of Au NP of various shapes and sizes.[6,8,9] Intense local heating using pulsed lasers has been shown to cause vesicle rupture,[10] which could allow drug delivery through membranes.[11] Importantly, the optical properties of tissue penetrating near-infrared (NIR) light are expected to be most useful in biological systems and can be used with Au nanorods (NRs) and nanoshells (NS), both of which have been used for heating and destruction of cells *in vivo* through high power laser exposure.[11−15] In this study, we aim to use lower powers in a nondestructive manner for controlled drug release.
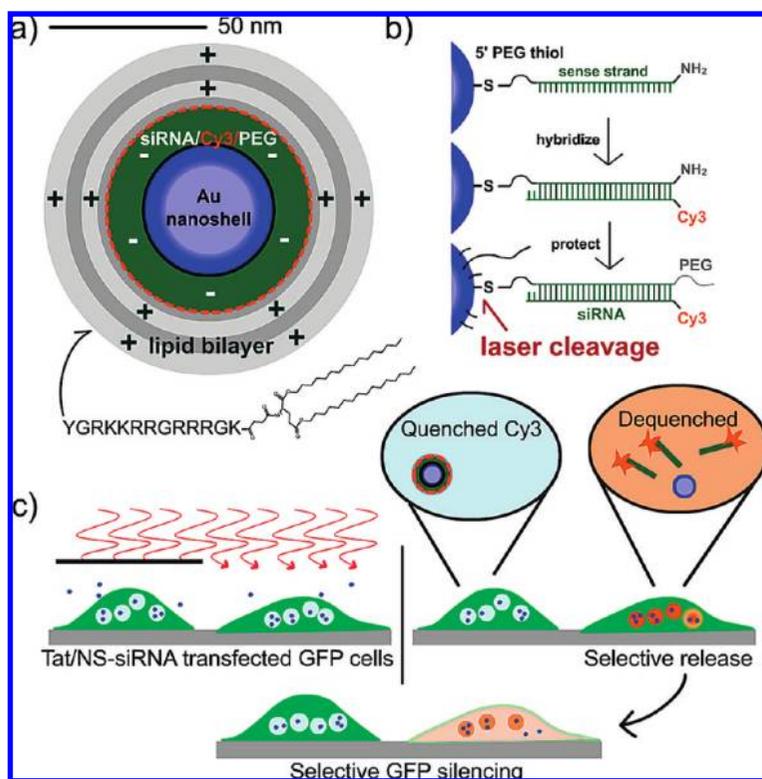
We have developed a novel architecture using ~40 nm hollow Au NS that provides temporally and spatially controlled cellular delivery of RNAi for gene

ABSTRACT The temporal and spatial control over the delivery of materials such as siRNA into cells remains a significant technical challenge. We demonstrate the pulsed near-infrared (NIR) laser-dependent release of siRNA from coated 40 nm gold nanoshells. Tat-lipid coating mediates the cellular uptake of the nanomaterial at picomolar concentration, while spatiotemporal silencing of a reporter gene (green fluorescence protein) was studied using photomasking. The NIR laser-induced release of siRNA from the nanoshells is found to be power- and time-dependent, through surface-linker bond cleavage, while the escape of the siRNA from endosomes occurs above a critical pulse energy attributed to local heating and cavitation. NIR laser-controlled drug release from functional nanomaterials should facilitate more sophisticated developmental biology and therapeutic studies.

KEYWORDS: nanoparticle · nanoshell · TAT · laser · gold · silencing · RNA

Figure 1. (a) Diagram of Tat-lipid-coated NS−siRNA used for transfection and selective release of siRNA. (b) Schematic of the siRNA construct used. The sense strand is composed of 5′ HS-(CH₂)₆-PEG₆-RNA-(CH₂)₆-NH₂, which is coated onto Au, hybridized, then backfilled with HS-PEG-NH₂, HS-(CH₂)₃SO₃, amines reacted with NHS-PEG₇-OCH₃. The 3′ Cy3 on the 27 base antisense strand is quenched due to proximity to gold. (c) Scheme of gene knockdown using laser. Transfection using the Tat-lipid allows uptake of NS−siRNA, followed by patterned exposure to release siRNA into the endosome volume or into the cytoplasm, and tracked using Cy3 dequenching upon release. After 1−2 days, laser-dependent GFP silencing is observed.

silencing, through a direct endosome release mechanism activated by pulsed laser treatment, and monitored by cyanine 3 (Cy3) dye fluorescence. A Tat peptide-lipid cell internalizing agent (Tat-lipid) allows the use of low NS concentrations and laser-dependent endosomal RNAi release. Controlling which subpopulation of cells will receive the nucleic acid at which time would enable developmental biology studies, which currently rely largely on passive chemical transfection methods.

Our goal of using RNAi to silence a particular subset of cells at a predetermined time using NS-based delivery requires that the NS respond to the light more or less predictably. RNAi requires a duplex RNA with certain limits on size and chemical modifications,[16] and Figure 1b describes the stepwise formation of the modified RNA on the NS, attached by a single cleavable Au−S bond. For simplicity, a single RNA is depicted, but in fact, the surface is tightly packed, beginning with the initial sense strand thiolate functionalization step. The combination of the gold−sulfur bond cleavage[6,8] and NS architecture is designed to allow the light-induced release of the siRNA. In contrast, mechanisms relying on thermal dehybridization have also been

used[1,17] but are anticipated to be less efficient for release of directly bound duplex RNA.

Recent cell studies have used nanomolar concentrations of NPs which can result in more than 10⁶ particles per cell.[18] We sought to minimize the need for high solution concentrations of NPs to minimize cost and unwanted impacts on cellular function. Cationic polymers and peptides can efficiently deliver particles into cells,[19] requiring only picomolar particle solution concentrations, given their high affinity with the cell surface.[19−23] In particular, nontoxic Tat peptide has been used to deliver NPs, protein, siRNA, or artificial vesicles into endosomes,[22−26] typically through direct NP conjugation or tethered to a lipid. Here we used a Tat-lipid conjugate, creating a peptide amphiphile[27−29] capable of self-assembling on the surface of our NS−siRNA assembly (Figure 1) and thus providing a high density of Tat per particle in a facile manner. The active complex is prepared through electrostatic assembly of highly cationic Tat-lipid around the anionic NS−siRNA, with membrane sealing to stabilize the complex, orient a second Tat layer outward for cellular binding, and, importantly, protect RNA from rapid degradation by enzymes. The RNA sequence was based off the EGFP-S1 Dicer substrate (IDT), previously shown to potently silence GFP,[30] and modified with necessary PEG thiol, amino, and Cy3 modifications, leaving the antisense 3′ unmodified for Dicer activity.[31]

The time-dependent intracellular fate of NPs is poorly understood, but parameters such as NP size and surface charge, as well as cell type, and transfection agent are likely to be important. In contrast to approaches in which time and spatial control are not sought,[2,32,33] intracellular fate is highly relevant to our NS−siRNA design. A major concern is the routing of NP into lysosomes *via* initial placement into endosomes, making any RNAi process ineffective due to enzymatic degradation and Au NS aggregation. Using the Tat-lipid conjugate is expected to prevent late endosome and lysosomal fusion, by directly stimulating the macropinocytosis endocytic pathway.[24,34,35] The temporary transfer of the NS−siRNA into more neutral pH and less degradative pinosomes should therefore provide a basis for temporal control over RNA release from the NS−siRNA into the cytosol and thus exert control over RNAi. Finally, given prior demonstration that irradiation of NS at NIR wavelengths leads to Au heating, microbubble cavitation, and liposome rupture,[10] we hypothesized that a collective NS−siRNA response to the pulsed laser would allow a fraction of endosomes to rupture, spilling their contents into the cytosol. We test this strategy with successful gene silencing, indeed correlated with cytosol release of Cy3 taking place near
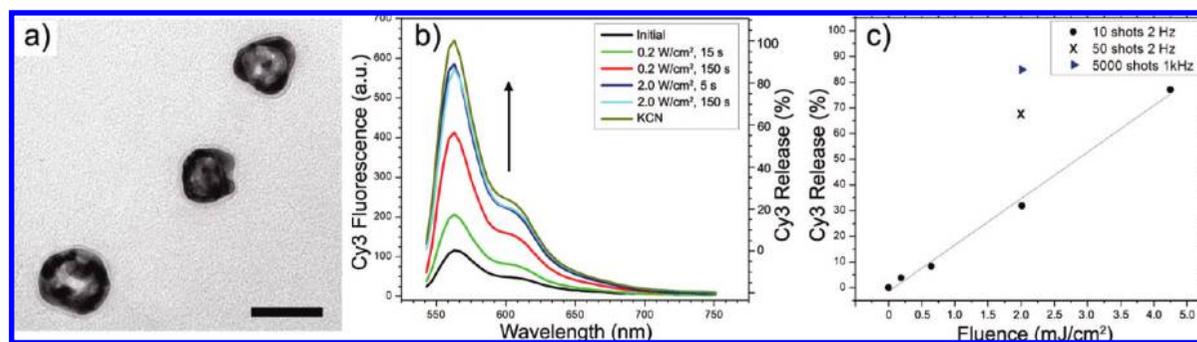
Figure 2. (a) TEM of Au NS coated with the sense strand RNA thiol. The ~40 nm Au shell is porous with a hollow core, formed by Au galvanic exchange initiating at the surface of Ag precurser nanoparticles. The RNA layer is visible as a light contrast shell, verified by focus series. Scale bar is 50 nm. **(b)** Release of siRNA−Cy3 from separate aliquots of NS−siRNA in buffer, tracked by the fluorescence increase of the solution upon release. A 5.5-fold increase in fluorescence is observed, indicating the Cy3 is quenched by ~80% initially. Note, maximum release by laser is ~90% the intensity for cyanide-etched sample. **(c)** Energy-dependent release after 10 shots (across fluence range). Samples at fixed fluence 2.0 mJ/cm^2 for 50 shots at 2 Hz and 5000 shots at 1 kHz show asymptotic release.

the previously established laser energy threshold necessary to induce cavitation.[10]

Hollow Au NS with a diameter of ~40 nm and ~3 nm thick shells, and with plasmon centered near 800 nm, were used for optimal excitation with the NIR pulsed laser (Figures 1 and 2a). After assembly of the RNAi onto the NS (Figure 1 and Methods), the surface was backfilled with passivating thiols and PEGylated using the amine attached to the outside terminus of the sense strand, stabilizing the conjugate against aggregation. After washing, the NS−siRNA were tested for release by irradiation using the femtosecond 800 nm pulsed laser, with a physical beam width of 2.3 or 5 mm (Gaussian intensity profile), at 2 or 1000 pulses per second, and variable power and exposure time. The observation of release was made possible by the 5′-positioned Cy3. The dye is partially quenched when near the gold,[36,37] while dequenching upon laser release may be observed separately from the green fluorescent protein (GFP) fluorescence.

The controllable increase in fluorescence at 1 kHz (Figure 2b) demonstrates that the monolayer of Cy3 is quenched up to 80%, normalized against a sample treated with KCN[2] (Figure 2b). The laser-mediated release was further examined using fluorescence microscopy. NS−siRNA were detectable as bright single particles with a dark background, attributed to the large number (10^2−10^3) of Cy3 bound to each Au NS, whereas after laser exposure, the solution itself became homogeneously fluorescent from released cargo (Supporting Information, Figures S1−S3).

Single laser shots resulted in detectable fluorescence release (10 shots, Figure 2c) and were used to further understand the relationship between energy input, exposure times, and release efficiency. When we assume a linear dependence, a slope of 1.76 ± 0.07% release per shot per mJ/cm^2 was found from 10 pulses at a rate of two per second. Thus, a dosed release is best executed at high power with a few shots or at low powers with higher pulse rate over multiple seconds. The re-

lease power dependency is similar when the dye is on either directly attached or hybridization-attached strands, indicating that release is not simply through local heating and subsequent dehybridization (Supporting Information, Figures S4 and S5). Our results are generally consistent with hot-electron-induced Au−S bond cleavage shown by El Sayed and co-workers on Au NPs coated with thiol−DNA.[8]

We used a GFP expressing cell line (mouse endothelial, C166-GFP) for reporting silencing efficiency.[36] Epifluorescence microscopy was used to determine the level of silencing using a filter set for GFP, with a Cy3 filter for verifying uptake and release of siRNA. Lipofectamine[38] has been used with NPs in several studies to facilitate transfection.[33,38] The complexation of Lipofectamine with anionic NS is efficient for facilitating uptake into endosomes, indicated by punctate Cy3 fluorescence scattered throughout the cytoplasm; yet, no cytosol release of NS was observed even after several days (data not shown). This may be due to the lack of passive transfer to the cytosol of the relatively large NS or NS clusters as compared with quantum dots[33] or small solid Au NPs,[2] that is, a consequence of too few NS per cell and inefficient particle escape. Translocation of high concentrations of NPs into the cytosol, although in our case most likely inefficient, could result in silencing due to potent RNAi activity. Furthermore, our use of Lipofectamine/NS−siRNA did not exhibit the expected changes in fluorescence after NIR pulsed release, either in solution or within cells, nor did we observe silencing (data not shown). This may be due to NS clustering, which directly changes the plasmon response, or altered diffusion of cleaved siRNA from the complex. Instead, we found the Tat-lipid conjugate superior to Lipofectamine for our purposes (Figure 1). Tat-lipid was able to coat the NS−siRNA (Figure 1a and Supporting Information, Figures S1−S3), which allowed efficient uptake into cells, controlled to be between ~10 and 10^3 NS per cell, while the nanostructure allowed laser release (Figure 3).
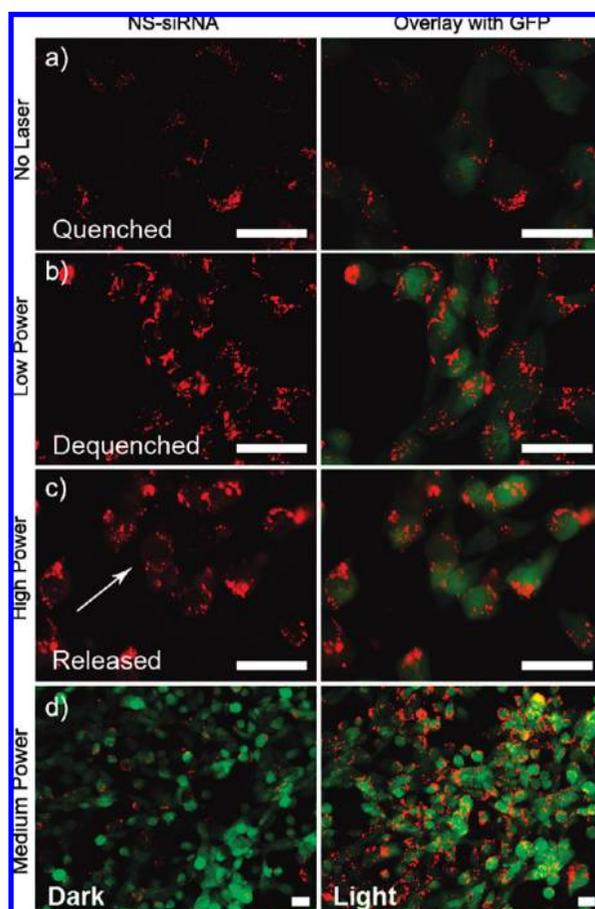
Figure 3. (a) NS—siRNA are observed inside cells, contained in endosomes, after Tat-lipid transfection into GFP expressing mouse endothelial cells. (b) Upon exposure for 20 s with 0.51 W/cm^2, the average brightness of the punctate vesicles increases. (c) Release of some Cy3—siRNA into cytosol is observed to occur at higher laser power (3.1 W/cm^2, 1 kHz). (d) Direct comparison at lower magnification (overlays) after exposure to 2.4 W/cm^2 (light) *versus* area with blocked laser (dark). Cultures were incubated for 1 h at 37 °C before imaging. Scale bars are 25 μm.

While laser-dependent siRNA release into endosomes is clearly evident by the increase in Cy3 fluorescence through dequenching, limited release into the cytosol was observed at the powers sufficient for homogeneous release in solution (*e.g.*, 0.2 W/cm^2, Figure 2b). We did not detect GFP silencing under this condition (Supporting Information, Figure S6b,c). The low laser powers (up to 2.4 W/cm^2 at 2 s, 1 kHz), which are clearly sufficient for free solution release (Figure 2b), when performed inside cells causes endosomes housing the NS—siRNA to simply increase their average intensity (red channel) by a factor of ~2–5 (Figure 3b,d and Supporting Information, Figure S7). The endosomes still exhibit high contrast against a dark cytoplasm background, indicating Cy3 trapping within sealed endosomes. Most importantly, at sufficiently high power (3.1 W/cm^2, 20 s), we observe the critical cytosolic release transition, discerned as a combination of a diffusely stained cytoplasm in many cells along with the brightening effect in the remaining endosomes (Figure 3c). We also observe changes in number, size,

and intensity of the remaining (punctate) endosomes. Achieving this endosome escape is deemed vital to the silencing properties of the siRNA from the NS conjugates using the Tat-lipid transfection method.

We used the combination of NS—siRNA release and NS-induced endosome rupture explored in Figure 3c and compared this with Lipofectamine RNAiMAX (Lipofectamine) transfection of control siRNA against GFP. We chose a power above the threshold expected to cause some diffuse cytosolic fluorescence (3.5 W/cm^2, 30 s). The GFP expressing mouse cells were seeded and transfected on day −1. Selected wells were irradiated on day 0 and imaged over the course of three additional days. NS—siRNA with no laser exposure (Figure 4b) exhibited high GFP expression no different than controls (Supporting Information, Figure S6). NS—siRNA with laser exposure showed obvious silencing by day 2 (Figure 4c). Lipofectamine silencing (Figure 4d) was observed by day 1, ~36 h after initial transfection. All samples showed high viability indicated by cell confluency, with cells doubling in population every day. The GFP levels were determined by pixel intensities on day 2 to be essentially equal, 80% silenced for laser-exposed NS—siRNA and 85% for Lipofectamine, relative to control, NS—siRNA without laser (Supporting Information, Figure S6). Negative control NS composed of 2′Ace-protected sense strand hybridized to antisense DNA—Cy3, prepared identically to the NS—siRNA, exhibited no silencing activity after laser exposure (Supporting Information, Figure S6). Furthermore, laser exposure of wells containing only cells indicated no photobleaching of GFP (Supporting Information, Figure S6). Notably, the same stock of NS—siRNA was used over several weeks of experiments with identical silencing efficiency.

Photomasking was examined by patterning the lid of the culture plate with a black pen (Figures 1c, 3d, and 5 and Supporting Information, Figure S8). The vertical beam passes through the clear region to expose the portion of the cell monolayer underneath. The cells imaged ~32 h later (Figure 5) showed ~50% silencing exclusively in the area exposed to the laser, as would be expected, and reached ~75% the next day (Supporting Information, Figure S8). The punctate Cy3 fluorescence was also dramatically reduced both in intensity per endosome and number of fluorescent endosomes in exposed regions, attributed to siRNA release and/or a dilution effect. We find this effect general for all laser-exposed cells compared to unexposed controls, indicating dispersal/degradation of siRNA after release from the NS surface (Figure 5b and Supporting Information, Figure S9). For cells exposed at low power with negligible cytosol release, the clearance of Cy3 may be due in part to exocytosis of pinosomes.[39,40]

To explore silencing at higher powers and shorter exposure times, a smaller 2.3 mm beam diameter was tested; 6.9 and 20.4 W/cm^2 with 2 s exposure at 1 kHz pulse rate under constant movement around the 5 mm

culture well showed the same maximum of ~80–85% silencing after 48 h with photomask patterning (Supporting Information, Figure S6). Lower powers of 0.9 and 2.9 W/cm^2 showed negligible silencing in this format (Supporting Information, Figure S6). The threshold power for silencing at the shorter 2 s exposure time was thus determined to lie between 2.9 and 6.9 W/cm^2, consistent with ~3.5 W/cm^2 using 30 s exposure and 5 mm beam (Figure 4) and slightly higher power than necessary for the 20 s exposure in Figure 5 (2.5 W/cm^2). We note that each well reached a similar confluency, indicating viability continues through 20 W/cm^2 (20 mJ/cm^2 per pulse, Supporting Information, Figure S6).

Our demonstration of time and spatially controlled RNAi-mediated gene silencing relies on the use of Tat-lipid modified Au NS through the release of siRNA from NS as well as the release of siRNA from endosomes; both release mechanisms are controlled by laser treatment. While Au NPs, NRs, and NS have been explored in their capacity to kill cells through plasma membrane disruption,[12,14] the powers are significantly higher than what is necessary for RNA release here with our NS–siRNA approach, and cells are more resistant to photothermal effects when the particles are internalized prior to laser exposure.[11] The high viability we observe is in accordance with a recent paper using a focused, scanned NIR pulsed laser and internalized nanorods. That study[11] found membrane blebbing to occur after ~10^4 pulses at energies of ~24 mJ/cm^2 per pulse, while we observe 70% RNA release after 50 pulses of 2 mJ/cm^2 in solution and 80% silencing from laser exposures of 3.5–20.4 mJ/cm^2 per pulse at 1 kHz for 2–30 s.

We identified a number of requirements for successful laser-induced gene silencing using NS. First, immobilization of RNA on NS requires at minimum a terminal thiol modification. A study with DNA on Au NPs showed that having PEG between the thiol and first nucleotide benefits the assembly.[41] Hypothetically, the laser pulse release does not depend on the length of the strand, such that having a linker could position the RNA further from the surface and shield it from the hot surface.[6] We found that ~50% of the sense strands could be hybridized under the chosen conditions and was not dependent on antisense concentration beyond a certain excess (data not shown). Since excess sense strand was not expected to interfere with RNAi, we settled on 50% as a decent balance.

Interestingly, during hybridization (Figure 1b), the NS tend to lightly aggregate, forming macroscale bluish-black flocculates visible to the naked eye and which appear highly fluorescent under the microscope due to the hybridized Cy3 strand. This issue was solved by installing a short amine-reactive PEG to terminate the duplex, whereby the solution returned to a highly dispersed state consisting of individually fluorescent NS
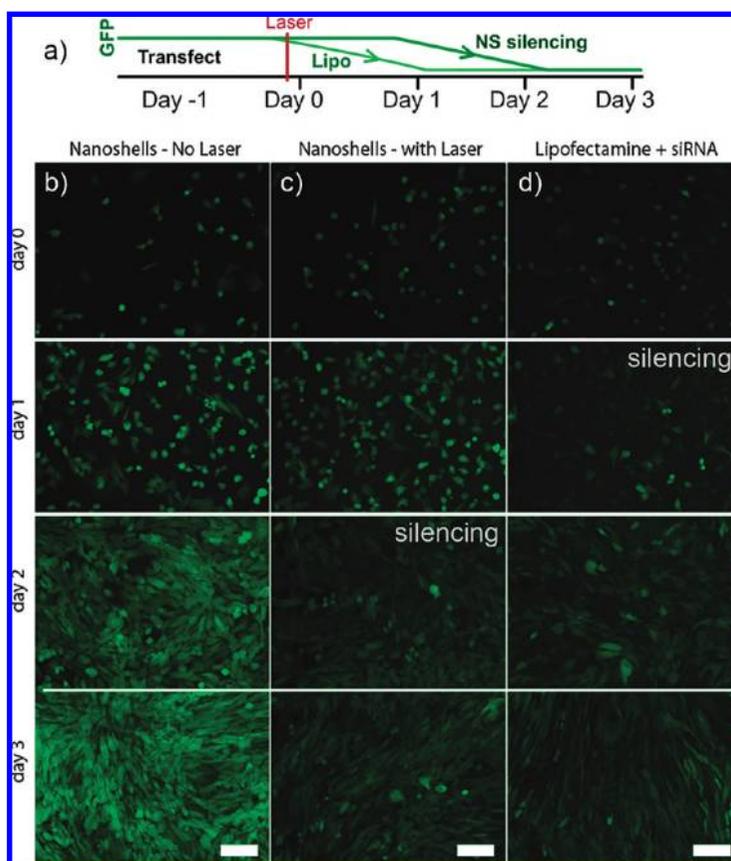
Figure 4. Laser-induced knockdown was compared to Lipofectamine delivery of control siRNA against GFP (IDT). (a) Timeline of events; Tat-lipid or Lipofectamine transfection of either NS–siRNA or siRNA, respectively, occurs on day −1. For Lipofectamine, the silencing process begins immediately and is complete after 2 days time, while for NS–siRNA, the laser is required, with similar 2 day progession. After overnight incubation with Tat-lipid/NS–siRNA (b,c) or Lipofectamine/ siRNA (d), NS–siRNA (in c only) were exposed to the pulsed laser (day 0, 3.5 W/cm^2, 30 s constant movement of 5 mm beam). Wells are compared over a period of 3 days. NS–siRNA with no laser showed full GFP expression throughout. Lipofectamine shows ~85% knockdown after day 1, while NS–siRNA exposed to laser show ~80% GFP reduction after day 2. High viability is indicated by the proliferation rate and morphology. Scale bars are 50 μm.

(Supporting Information, Figure S1). Although this layering system could be further optimized, we found that NS–siRNA prepared in this fashion could be used over at least several weeks for reproducible knockdown experiments. For convenience, the sense strand–NS stock is stored for longer periods, and aliquots are hybridized with antisense as needed.

An important stage of development consisted of controlling cellular uptake of the NS and optimizing laser release in a cellular context. We initially tested Lipofectamine-based delivery, known for condensing nucleic acids into compact nanoparticles without much toxicity,[38] but it did not allow normal laser release. We explored the use of a Tat peptide lipid conjugate to deliver the NS without interfering with laser release. Tat is a commonly used stimulator of macropinocytosis,[24] resulting after electrostatic binding to the anionic cell surface glycans. The assembly could be tuned from picomolar to nanomolar NS–siRNA particle concentration, remarkably with minimal aggregation (color shift) in solution, pre-
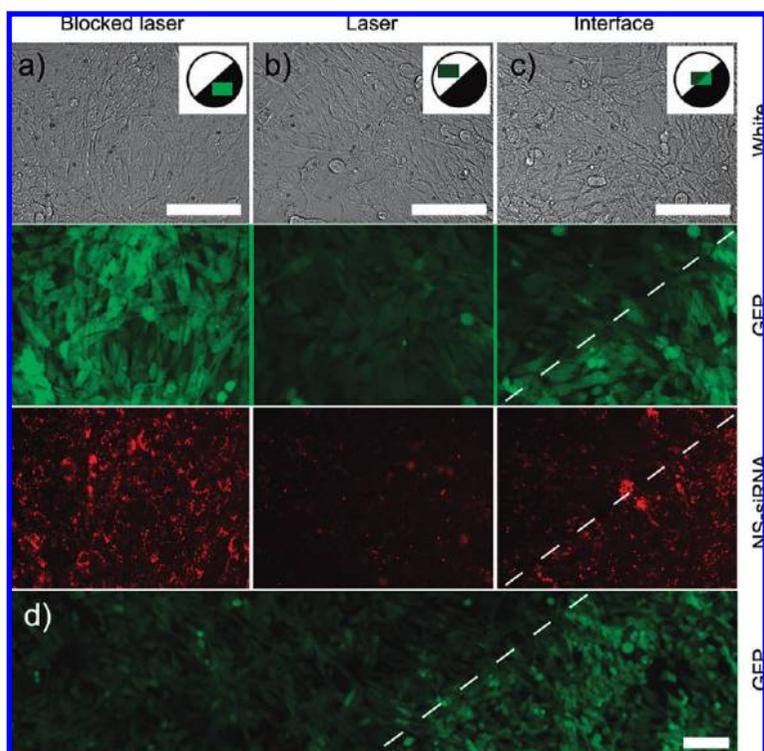
Figure 5. Patterned exposure by blocking one-half of the beam (2.5 W/cm^2, 20 s) as it passed through the lid and illuminated the 5 mm diameter well containing cells. Imaging ~32 h later shows the regiospecific knockdown of GFP. (a) Cells and NS−siRNA in a region blocked by the mask show high GFP and continued punctate Cy3 staining. (b) In exposed cells, there is a drop in GFP and the Cy3 is diffuse, with fewer puncta. (c) Imaging the interface between exposed and not exposed regions. The white dashed line indicates the border of knockdown, corresponding to the pattern edge. Scale bar is 50 μm. (d) Lower magnification image of the interface. Scale bar is 100 μm.

sumably through electrostatic repulsion of Tat-coated surfaces. Immobilization experiments on glass (Supporting Information, Figures S2 and S3) allowed us to conclude that isolated NS and small aggregates (<~1 μm) released their RNA−Cy3 into the bulk solution with expected laser power dependency. Larger aggregates tended to remain intact after laser treatment (Supporting Information, Figure S3b), highlighting the importance of aggregation state.

While Tat-lipid provides a route to controllably deliver the intact, laser-responsive NS−siRNA into endosomes, we did not observe NS free in the cytosol prior to laser exposure. Dynamic, punctate fluorescence was observed over several days time (Supporting Information, Figure S9a,c), indicating trafficking of the vesicles containing trapped NS−siRNA. Knockdown was not observed without laser exposure, even when excess free siRNA was coassembled with the Tat-lipid (data not shown). In control experiments, such a noncovalent assembly format did induce knockdown when assembled using Lipofectamine, although those experiments exhibited slight cytoplasmic diffuse fluorescence in addition to the endosome-trapped NP or NS cores. Lipofectamine knockdown is thought to occur through a membrane mixing process, that is, transfer of siRNA passively from the outer

parts of the polyplex through the endosome membrane; however, the Tat-lipid does not function this way. We thus anticipate that future applications of NS could allow delivery of a variety of noncovalently bound molecules, transferred to cytosol through NS/laser-induced endosome rupture. Alternatively, lipid formulations could have components with membrane disrupting qualities; ideally, an agent for releasing intact NS conjugates into the cytosol would allow more sophisticated regiospecific (subcellular) localization of cargo release, at very low powers, in a dosed manner.

Our prior work showed NS heating can cause rapid liposome rupture, with a threshold of ~2.3 J/cm^2 per pulse.[10] Consistent with this, we show that the threshold for RNAi-dependent silencing and the diffuse cytosol staining in some cells is ~3 W/cm^2 (Figures 3, 5, and Supporting Information, Figure S6). At ever higher powers, NS structural changes occur which include collapse, melting, or fragmentation into solid Au NPs with a new red plasmon resonance (500−600 nm, Supporting Information, Figure S10).[10,42] Taken together, the silencing observed in this study is best attributed to cavitation effects on the local endosome membrane causing leakage or popping, thereby releasing siRNA into cytosol for RNAi, although other mechanisms are possible. Exposures above this power threshold offer no clear advantages in silencing efficacy (Supporting Information, Figure S6). In contrast, the release of siRNA from the surface into the endosome volume (without rupture) can occur at lower powers (e.g., 0.51 W/cm^2 Figure 3b,d) yet this is not sufficient to cause GFP silencing (Supporting Information, Figure S6, 0.9 W/cm^2).

The effect of average power versus peak energy fluence is important for controlling the locality of the thermal effects.[8,43,44] In one regime, continuous wave excitation can be used to set up a relatively stable nanoparticle−solvent thermal relationship, whereby the Au core is slightly hotter than the surrounding dissipating liquid (but unable to cavitate or melt), and continued irradiation causes the bulk solvent to rise in temperature from the deposited energy.[13−15] Continuous wave heating creates a nanoscale gradient which can be used to selectively heat material near the surface.[1] While such a gradient may be able to increase the desorption rate of hybridized oligos, the rapid cleavage of near-covalent bonds such as thiol−Au would require a higher peak Au temperature, more easily executed using pulsed lasers. El Sayed et al. attributed pulsed laser release of thiol DNA on Au NPs to hot electrons from the Au plasmons destabilizing gold−thiol bonds before the electrons have thermalized with the lattice of the material, or through vibrational stresses, occurring before transfer of heat to the surrounding fluid.[8] This electrochemical effect is an attractive release technique

due to simplified requirements for directly bound S atoms though extremely localized temperature change. Pulsed laser absorption and ablation has been the subject of a number of modeling studies,[44−46] usually on solid Au NPs or NRs in water. A sharp exponential decrease of temperature away from NP surface is generally predicted, such that short-term temperature differentials of >200 °C may be set up between at-surface and the solution ~5 nm away.[44] The selective heating of the surface bonds using pulsed lasers should facilitate release for a wide arsenal of attached cargo. While the laser cleavage site(s) in the thiol−PEG linker is not directly verified in this study, we note that in control studies short thiol single-stranded oligos are also released efficiently (Supporting Information, Figures S4 and S5), consistent with recent reports.[6,8] It should be considered that general molecular cargos may exhibit heat-induced degradation upon release, which could negatively impact drug efficacy (although the time spent at elevated temperatures will be on the nanosecond time scale).[8,44,47] Linker length optimization and anchor group affinity could thus be an important design aspect, and future studies are underway to understand the release process in more detail.

In summary, we show gene silencing in a temporally and spatially controlled manner through a NS-activated release of siRNA using pulsed NIR laser. Integral to the approach was to first obtain cytoplasmic uptake of particles through complexation with Tat-lipid, allowing rapid uptake of low concentration NS−siRNA (~10 pM). However, we found that endosome membranes efficiently retain released RNA, observed through dequenching of punctate Cy3, unless endosome rupture is caused by more disruptive NS heating. In the latter case, a change from punctate to diffuse fluorescence occurred due to cytosol release, which was correlated with gene silencing. We attribute the full effect to heat or cavitation-induced endosomal membrane disruption and siRNA diffusion into cytosol. The combination of surface release and endosome rupture enabled silencing approximately equal to Lipofectamine transfection. While the popping requirement is a drawback since it is not required for the cargo release step itself, the cells survive the process with vigor. We anticipate that, given the main requirement for release being the resonance between the plasmon of the nanomaterial and the pulsed laser, a variety of uniquely resonant nanoshells, nanorods, and nanoparticles could ultimately result in multiplexed subcellular delivery given highly focused pulsed lasers. Needless to say, more advanced transfection methods which overcome the endosome barrier would be highly enabling for NP-based drug delivery.

METHODS

Nanoshell Synthesis. Hollow gold nanoshells were prepared as described previously.[10,42] Silver seed nanoparticles were prepared by reducing a well-stirred solution of 600 mL of 0.2 mM AgNO$_3$ with 0.6 mL of 1.0 M NaBH$_4$ in the presence of 0.5 mM sodium citrate in deionized water (DI). The solution was stirred for several hours to allow NaBH$_4$ to fully hydrolyze. Larger silver nanoparticles to be used as sacrificial templates for the gold nanoshells were grown from the silver seed solution by adding 0.6 mL of 2.0 M NH$_2$OH HCl and 1.5 mL of 0.1 M AgNO$_3$ and stirring overnight. Galvanic replacement of silver with gold was performed by quickly mixing 3.8 mL of 25 mM HAuCl$_4$ solution with the silver nanoparticles at 60 °C. The volume added was optimized for an absorbance peak at 800 nm. Particle concentration was estimated at ~1 nM, with extinction of 0.1 at the peak ~800 nm, 0.1 cm path length. The solution was cooled to room temperature and kept in the dark for at least several days before use.

Sense RNA Preparation. The sequence of siRNA was based off the potent siRNA against the EGFP gene (IDT EGFP-S1 DS positive control), an asymmetric duplex having a 2-base 3′-overhang on the antisense strand two 3′-DNA residues on the sense blunt end (termed EGFPS1 R 25D/27).[30] Fifty nanomole sense strand RNA (Dharmacon), 5′-HO-(CH$_2$)$_6$-SS-(CH$_2$)$_6$-spacer18-ACCCUGAAGUU-CAUCUGCACCACdCdG-(CH$_2$)$_6$-NH$_2$, dCdG indicating deoxynucleotides, was purchased from Dharmacon. The oligo was first 2′Ace-deprotected using the recommended 30 min incubation at 60 °C in pH 3.8 buffer supplied with the oligo and split into tubes with 3.1 nmol each then lyophilized. Each tube is enough for at coating at least 1 mL of NS citrate, and 1 mL of ~1 nM NS can silence 1000 wells (96-well format). To reduce the disulfide, the RNA was brought up in 50 μL of water and Tris(2-carboxyethyl)phosphine HCl pH 7.0 (TCEP, 0.5 M, #646547-10 × 1 ML, Sigma) was added to 5 mM. After 10 min, CHCl$_3$ was added and mixed to extract the mercaptohexanol (which as a free thiol can interfere with the NS functionalization). The aqueous layer was collected and used immediately.

NS-Sense Preparation. Citrate-stabilized NS solution contains excess Ag$^+$ and AgCl solids which settle to the bottom over several days. In a typical synthesis of NS−siRNA, NS (3 mL) were removed and placed in a 20 000 MWCO Slide-a-Lyzer (Pierce) in 1500 mL of 500 μM citrate buffer at pH 5.5. One milliliter of diethylpyrocarbonate (DEPC) was added to sterilize and neutralize any RNase activity, and stirring for 2 days at room temperature allows the DEPC to decompose. Note that autoclaving blue shifts the plasmon peak toward 600 nm, indicating structural changes. The ~1 nM NS were combined with freshly reduced thiol RNA (3 μM in 5 mM TCEP pH 7.0), sonicated, and stored overnight at 4 °C. The next day the solution was sonicated and salted to 60 mM Na$^+$ using 3.0 M NaCl, 0.3 M Na citrate pH 7.0 solution (20× SSC, RNase free, Invitrogen) to increase RNA density on the NS. Sonication and overnight incubation followed at 4 °C. The process was repeated until 180 mM Na$^+$ was reached for at least 18 h. A portion of the blue NS-sense conjugates was isolated for characterization by centrifuging at 6000 rpm for 10 min and dispersing at least three times with 30 mM HEPES, 100 mM Na acetate pH 7.5 (DB, Duplex Buffer, IDT). Successful functionalization is indicated by presence of strong 800 nm plasmon peak and a distinct RNA band at 260 nm over the broad absorption of NS in that region. Notably, NS without the RNA layer are unstable in DB, forming large aggregates.

NS−siRNA. Antisense strand 5′-CGGUGGUGCAGAU-GAACUUCAGGGUCA-Cy3 (all RNA, IDT) or control strand of equivalent sequence DNA−Cy3 (IDT) was added at 5 μM to an unwashed (or washed) stock of 300 μL NS-sense and incubated at 37 °C for 1 h with periodic sonication, then incubated overnight at 4 °C. Note, the NS tend to slowly fall out of solution upon duplex formation. The following day, 15 μL of 80 mg/mL PEG 8 kDa in ethanol/DB 80/20% was added to help disperse the NS, sonicated, then thiol−PEG−amine in ethanol/DB (3 kDa, Rapp Polymere) was added at 100 μM to backfill any large exposed surface sites. The NS remain aggregation prone, especially at 4 °C, indicating that the surface is tightly packed with dsRNA. After 1 h, HS(CH$_2$)$_3$SO$_3$Na in DB was added at 30 μM for passivating smaller surface sites. After 1 h, the NS−siRNA were centrifuged and washed with DB. The ter-

minal amines were then reacted with NHS-PEG$_7$-OCH$_3$, ~6 mM (MW ~ 509, Quanta Biodesign, NHS is N-hydroxysuccinimide ester) with periodic sonication for 1 h at room temperature. The completed NS–siRNA were stable in solution and retained a plasmon peak at 750–800 nm. Centrifugation and washing 2–3 times with cold DB containing 0.1 mg/mL PEG 8 kDa, with added 1% Hanks buffer salt solution (HBSS, with Mg^{2+} and Ca^{2+}), was performed to remove excess antisense (HBSS for divalent cation stabilization of duplex). This solution was passed through a 0.22 μm syringe filter (Millex-GV, PVDF sterile 4 mm, #SLGV004SL) used for knockdown for several weeks when stored at 4 °C (sonicated briefly before use). Individual particles are easily observed by epifluorescence microscopy at 100× magnification oil immersion lens under Cy3 excitation, at 80 ms integration, and gain of 1 (Olympus BX-41).

Tat-Lipid. Tat peptide was purchased from Anaspec (San Jose, CA), fully protected on the resin; sequence Tyr-Gly-Arg-Lys-Lys-Arg-Arg-Gln-Arg-Arg-Arg-Gly-Lys-OH. The peptide corresponds to a sequence derived from HIV-1 trans-activator protein (TAT$_{47-57}$) onto which a glycine and a lysine with a Dde protecting group have been added on the C-terminus. The dialkyl lipid acid 4-(1,5-bis(hexadecyloxy)-1,5-dioxopentan-2-ylamino)-4-oxobutanoic (diC16) was synthesized as described previously.[48] Coupling of the lipid tail on the ε-amine of the C-terminal lysine of Tat peptide was performed on the resin using standard Fmoc chemistry. Following cleavage from the resin, the peptide amphiphile was purified using high-pressure liquid chromatography (HPLC; Shimadzu Corporation) on a reverse-phase Luna C8 column (Phenomenex), with gradients of acetonitrile (EMD chemicals, HPLC grade) in water containing 0.1% trifluoroacetic acid (Sigma). Identity of product was verified by electrospray ionization mass spectrometry, and purity was determined using analytical HPLC on a reverse-phase Luna C8 column (Phenomenex). Material of purity greater than 95% was stored dry at −20 °C until used. The chemical structure of the peptide amphiphile used in this study is given in Supporting Information, Scheme S1. Stock solutions of the product were prepared by dissolving in DI at a concentration of 2 mg/mL, aliquoted, and stored at −20 °C for up to 2 months time before use with NS–siRNA.

Cell Culture. The mouse cell line C166-GFP (ATCC CRL-2581) is stably transfected with a plasmid reporter vector, pEGFP-N1 (Clontech), encoding enhanced green fluorescent protein (GFP). Cells were grown in RPMI-1640 medium (Sigma) supplemented with L-glutamine, 200 μg/mL Geneticin G418 selective antibiotic (Invitrogen), 10% fetal bovine serum, without phenol red, at 37 °C in 5% CO$_2$ in 6-well or 96-well culture plates (Corning 3595); 100 μL media for 96-well samples.

Tat-Lipid NS–siRNA Assembly and Transfection. Tat-lipid in water (11 μL, 2 mg/mL) was diluted in 100 μL of DB, and 30 μL of 80 μg/mL PEG 8 kDa (in 80% ethanol, 20% DB) was added. This supplied ~15% ethanol, which interferes with liposome formation until adding to NS–siRNA, which dilutes the ethanol. Ten microliters of ~ 500 pM NS–siRNA (~0.05 absorbance at 800 nm, 0.1 cm path length, NanoDrop 1000) was first combined with 10 μL of DB, and 1 μL of Tat-lipid solution was added and incubated for several minutes. Cy3 microscopy at 100× indicated isolated NS–siRNA and small clusters, with high avidity toward anionic glass surface due to the cationic lipid coating. One to ten microliters of this solution is added per 100 μL of media in a 96-well containing 0.9 × 10^4 cells, seeded >5 h prior (minimum of 10^{-11} M NS–siRNA, 10^{-9} M siRNA, 10^{-7} M Tat-lipid). After ~3 h to overnight incubation, the cells show NS concentration dependence uptake of 10–10^4 per cell, visible inside vesicles in a punctate Cy3 fluorescence pattern. Uptake into the cytoplasm and near the nucleus was observed, but NS were excluded from the nucleus itself. This fluorescence pattern persists for >3 days of cell growth (at one doubling per day), or until laser had released the siRNA in which case intensity increased immediately, then decreased dramatically by the following day. Lipofectamine RNAiMAX (Lipofectamine, Invitrogen) was used as a control with siRNA (IDT EGFP-S1 DS Positive Control); 0.5 μL of Lipofectamine was added to 50 μL of Opti-MEM (Invitrogen) and combined with 50 μL of Opti-MEM containing 0.5 μL of 5 μM siRNA and 0.5 μM siGLO Red tracker (Dharmacon). After 15 min, 5 μL was added per 100 μL media with serum.

Femtosecond Laser. The samples were irradiated by the output of the femtosecond (fs) Ti:sapphire regenerative amplifier (Spectra-physics Spitfire) running with 1 kHz repetition rate. The laser beam was collimated by a Galilean telescope to achieve a Gaussian diameter of 2.3 mm. In experiments without collimation, the full beam diameter was ~5 mm. Pulse duration was monitored by a home-built single-shot optical autocorrelator and was kept at about 130 fs. The spectral fwhm of the laser radiation was ~12 nm centered around 800 nm. The laser beam was directed onto the sample by a system of mirrors, and no focusing optics were used. The energy of the optical pulse was controlled by Schott neutral density glass filters. A thermopile power meter (Newport Inc., Irvine, CA) was used to measure the incident optical power.[10,42]

Laser Exposure. After >3 h incubation of cells with NS–siRNA, the medium was optionally replaced with fresh and plate sealed with parafilm. The 800 nm pulsed laser with a spot diameter of 5 mm or 2.3 mm was reflected by a mirror as a vertical beam into the culture plate (96-wells with 5 mm well diameter) aligned underneath. The plastic lid minimally absorbs at this wavelength, modified by marker pattern which absorbs strongly. Variable time and powers were chosen, and best results occurred when moving the plate to average the power. The cells were placed back in the 5% CO$_2$ 37 °C incubator for at least 1 h before imaging.

Supporting Information Available: Chemical structure of Tat-lipid. Additional figures. This material is available free of charge *via* the Internet at http://pubs.acs.org.

REFERENCES AND NOTES

1. Lee, S. E.; Liu, G. L.; Kim, F.; Lee, L. P. Remote Optical Switch for Localized and Selective Control of Gene Interference. *Nano Lett.* **2009**, *9*, 562–570.

2. Giljohann, D. A.; Seferos, D. S.; Prigodich, A. E.; Patel, P. C.; Mirkin, C. A. Gene Regulation With Polyvalent SiRNA–Nanoparticle Conjugates. *J. Am. Chem. Soc.* **2009**, *131*, 2072–2073.

3. Banerjee, D.; Slack, F. Control of Developmental Timing by Small Temporal RNAs: A Paradigm for RNA-Mediated Regulation of Gene Expression. *Bioessays* **2002**, *24*, 119–129.

4. Young, D. D.; Lusic, H.; Lively, M. O.; Yoder, J. A.; Deiters, A. Gene Silencing in Mammalian Cells With Light-Activated Antisense Agents. *Chembiochem* **2008**, *9*, 2937–2940.

5. Young, D. D.; Deiters, A. Photochemical Control of Biological Processes. *Org. Biomol. Chem.* **2007**, *5*, 999–1005.

6. Wijaya, A.; Schaffer, S. B.; Pallares, I. G.; Hamad-Schifferli, K. Selective Release of Multiple DNA Oligonucleotides From Gold Nanorods. *ACS Nano* **2009**, *3*, 80–86.

7. Chen, C. C.; Lin, Y. P.; Wang, C. W.; Tzeng, H. C.; Wu, C. H.; Chen, Y. C.; Chen, C. P.; Chen, L. C.; Wu, Y. C. DNA–Gold Nanorod Conjugates for Remote Control of Localized Gene Expression by Near Infrared Irradiation. *J. Am. Chem. Soc.* **2006**, *128*, 3709–3715.

8. Jain, P. K.; Qian, W.; El Sayed, M. A. Ultrafast Cooling of Photoexcited Electrons in Gold Nanoparticle-Thiolated DNA Conjugates Involves the Dissociation of the Gold–Thiol Bond. *J. Am. Chem. Soc.* **2006**, *128*, 2426–2433.

9. Chen, J.; Wiley, B.; Li, Z.-Y.; Campbell, D.; Saeki, F.; Cang, H.; Au, L.; Lee, J.; Li, X.; Xia, Y. Gold Nanocages: Engineering Their Structure for Biomedical Applications. *Adv. Mater.* **2005**, *17*, 2255–2261.

10. Wu, G. H.; Milkhailovsky, A.; Khant, H. A.; Fu, C.; Chiu, W.; Zasadzinski, J. A. Remotely Triggered Liposome Release by Near-Infrared Light Absorption *via* Hollow Gold Nanoshells. *J. Am. Chem. Soc.* **2008**, *130*, 8175–8177.

11. Tong, L.; Zhao, Y.; Huff, T. B.; Hansen, M. N.; Wei, A.; Cheng, J. X. Gold Nanorods Mediate Tumor Cell Death by Compromising Membrane Integrity. *Adv. Mater.* **2007**, *19*, 3136–3141.

12. Yao, C. P.; Rahmanzadeh, R.; Endl, E.; Zhang, Z. X.; Gerdes, J.; Huttmann, G. Elevation of Plasma Membrane Permeability by Laser Irradiation of Selectively Bound Nanoparticles. *J. Biomed. Opt.* **2005**, *10*, 64012–64019.

13. Choi, M. A Cellular Trojan Horse for Delivery of Therapeutic Nanoparticles into Tumors. *Nano Lett.* **2007**, *7*, 3759–3765.

14. Hirsch, L. R; Stafford, R. J; Bankson, J. A; Sershen, S. R; Rivera, B; Price, R. E; Hazle, J. D; Halas, N. J; West, J. L. Nanoshell-Mediated Near-Infrared Thermal Therapy of Tumors Under Magnetic Resonance Guidance. *Proc. Natl. Acad. Sci. U.S.A.* **2003**, *100*, 13549–13554.

15. Loo, C.; Lowery, A.; Halas, N.; West, J.; Drezek, R. Immunotargeted Nanoshells for Integrated Cancer Imaging and Therapy. *Nano Lett.* **2005**, *5*, 709–711.

16. Chiu, Y. L.; Rana, T. M. RNAi in Human Cells: Basic Structural and Functional Features of Small Interfering RNA. *Mol. Cell* **2002**, *10*, 549–561.

17. Hamad-Schifferli, K.; Schwartz, J. J.; Santos, A. T.; Zhang, S. G.; Jacobson, J. M. Remote Electronic Control of DNA Hybridization Through Inductive Coupling to an Attached Metal Nanocrystal Antenna. *Nature* **2002**, *415*, 152–155.

18. Giljohann, D. A.; Seferos, D. S.; Patel, P. C.; Millstone, J. E.; Rosi, N. L.; Mirkin, C. A. Oligonucleotide Loading Determines Cellular Uptake of DNA-Modified Gold Nanoparticles. *Nano Lett.* **2007**, *7*, 3818–3821.

19. Oyelere, A. K.; Chen, P. C.; Huang, X. H.; El Sayed, I. H.; El Sayed, M. A. Peptide-Conjugated Gold Nanorods for Nuclear Targeting. *Bioconjugate Chem.* **2007**, *18*, 1490–1497.

20. Thurn, K. T.; Brown, E. M. B.; Wu, A.; Vogt, S.; Lai, B.; Maser, J.; Paunesku, T.; Woloschak, G. E. Nanoparticles for Applications in Cellular Imaging. *Nanosci. Res. Lett.* **2007**, *2*, 430–441.

21. El Sayed, A.; Khalil, I. A.; Kogure, K.; Futaki, S.; Harashima, H. Octaarginine- and Octalysine-Modified Nanoparticles Have Different Modes of Endosomal Escape. *J. Biol. Chem.* **2008**, *283*, 23450–23461.

22. Tkachenko, A. G.; Xie, H.; Liu, Y. L.; Coleman, D.; Ryan, J.; Glomm, W. R.; Shipton, M. K.; Franzen, S.; Feldheim, D. L. Cellular Trajectories of Peptide-Modified Gold Particle Complexes: Comparison of Nuclear Localization Signals and Peptide Transduction Domains. *Bioconjugate Chem.* **2004**, *15*, 482–490.

23. Torchilin, V. P; Rammohan, R; Weissig, V; Levchenko, T. S. TAT Peptide on the Surface of Liposomes Affords Their Efficient Intracellular Delivery Even at Low Temperature and in the Presence of Metabolic Inhibitors. *Proc. Natl. Acad. Sci. U.S.A.* **2001**, *98*, 8786–8791.

24. Chen, B.; Liu, Q. L.; Zhang, Y. L.; Xu, L.; Fang, X. H. Transmembrane Delivery of the Cell-Penetrating Peptide Conjugated Semiconductor Quantum Dots. *Langmuir* **2008**, *24*, 11866–11871.

25. Caron, N. J.; Quenneville, S. P.; Tremblay, J. P. Endosome Disruption Enhances the Functional Nuclear Delivery of Tat-Fusion Proteins. *Biochem. Biophys. Res. Commun.* **2004**, *319*, 12–20.

26. Chiu, Y. L.; Ali, A.; Chu, C. Y.; Cao, H.; Rana, T. M. Visualizing a Correlation between siRNA Localization, Cellular Uptake, and RNAi in Living Cells. *Chem. Biol.* **2004**, *11*, 1165–1175.

27. Bitton, R.; Schmidt, J.; Biesalski, M.; Tu, R.; Tirrell, M.; Bianco-Peled, H. Self-Assembly of Model DNA-Binding Peptide Amphiphiles. *Langmuir* **2005**, *21*, 11888–11895.

28. Yu, Y. C.; Berndt, P.; Tirrell, M.; Fields, G. B. Self-Assembling Amphiphiles for Construction of Protein Molecular Architecture. *J. Am. Chem. Soc.* **1996**, *118*, 12515–12520.

29. Missirlis, D.; Khan, H.; Tirrell, M. Mechanisms of Peptide Amphiphile Internalization by SJSA-1 Cells *In Vitro*. *Biochemistry* **2009**, *48*, 3304–3314.

30. Rose, S. D.; Kim, D. H.; Amarzguioui, M.; Heidel, J. D.; Collingwood, M. A.; Davis, M. E.; Rossi, J. J.; Behlke, M. A. Functional Polarity is Introduced by Dicer Processing of Short Substrate RNAs. *Nucleic Acids Res.* **2005**, *33*, 4140–4156.

31. Kim, D. H.; Behlke, M. A.; Rose, S. D.; Chang, M. S.; Choi, S.; Rossi, J. J. Synthetic dsRNA Dicer Substrates Enhance RNAi Potency and Efficacy. *Nat. Biotechnol.* **2005**, *23*, 222–226.

32. Patel, P. C; Giljohann, D. A; Seferos, D. S; Mirkin, C. A. Peptide Antisense Nanoparticles. *Proc. Natl. Acad. Sci. U.S.A.* **2008**, *105*, 17222–17226.

33. Derfus, A. M.; Chen, A. A.; Min, D. H.; Ruoslahti, E.; Bhatia, S. N. Targeted Quantum Dot Conjugates for SiRNA Delivery. *Bioconjugate Chem.* **2007**, *18*, 1391–1396.

34. Ruan, G.; Agrawal, A.; Marcus, A. I.; Nie, S. Imaging and Tracking of Tat Peptide-Conjugated Quantum Dots in Living Cells: New Insights into Nanoparticle Uptake, Intracellular Transport, and Vesicle Shedding. *J. Am. Chem. Soc.* **2007**, *129*, 14759–14766.

35. Falcone, S.; Cocucci, E.; Podini, P.; Kirchhausen, T.; Clementi, E.; Meldolesi, J. Macropinocytosis: Regulated Coordination of Endocytic and Exocytic Membrane Traffic Events. *J. Cell Sci.* **2006**, *119*, 4758–4769.

36. Rosi, N. L.; Giljohann, D. A.; Thaxton, C. S.; Lytton-Jean, A. K. R.; Han, M. S.; Mirkin, C. A. Oligonucleotide-Modified Gold Nanoparticles for Intracellular Gene Regulation. *Science* **2006**, *312*, 1027–1030.

37. Seferos, D. S.; Giljohann, D. A.; Hill, H. D.; Prigodich, A. E.; Mirkin, C. A. Nano-Flares: Probes for Transfection and mRNA Detection in Living Cells. *J. Am. Chem. Soc.* **2007**, *129*, 15477–15479.

38. Zhao, M.; Yang, H.; Jiang, X. J.; Zhou, W.; Zhu, B.; Zeng, Y.; Yao, K. T.; Ren, C. P. Lipofectamine RNAiMAX: An Efficient siRNA Transfection Reagent in Human Embryonic Stem Cells. *Mol. Biotechnol.* **2008**, *40*, 19–26.

39. Panyam, J.; Labhasetwar, V. Dynamics of Endocytosis and Exocytosis of Poly(D,L-Lactide-*co*-Glycolide) Nanoparticles in Vascular Smooth Muscle Cells. *Pharm. Res.* **2003**, *20*, 212–220.

40. Chithrani, B. D.; Chan, W. C. W. Elucidating the Mechanism of Cellular Uptake and Removal of Protein-Coated Gold Nanoparticles of Different Sizes and Shapes. *Nano Lett.* **2007**, *7*, 1542–1550.

41. Hurst, S. J.; Lytton-Jean, A. K. R.; Mirkin, C. A. Maximizing DNA Loading on a Range of Gold Nanoparticle Sizes. *Anal. Chem.* **2006**, *78*, 8313–8318.

42. Prevo, B. G.; Esakoff, S. A.; Mikhailovsky, A.; Zasadzinski, J. A. Scalable Routes to Gold Nanoshells With Tunable Sizes and Response to Near-Infrared Pulsed-Laser Irradiation. *Small* **2008**, *4*, 1183–1195.

43. Huang, X. H.; Jain, P. K.; El Sayed, I. H.; El Sayed, M. A. Determination of the Minimum Temperature Required for Selective Photothermal Destruction of Cancer Cells with the Use of Immunotargeted Gold Nanoparticles. *Photochem. Photobiol.* **2006**, *82*, 412–417.

44. Volkov, A. N.; Sevilla, C.; Zhigilei, L. V. Numerical Modeling of Short Pulse Laser Interaction With Au Nanoparticle Surrounded by Water. *Appl. Surf. Sci.* **2007**, *253*, 6394–6399.

45. Pustovalov, V. K. Theoretical Study of Heating of Spherical Nanoparticle in Media by Short Laser Pulses. *Chem. Phys.* **2005**, *308*, 103–108.

46. Ekici, O.; Harrison, R. K.; Durr, N. J.; Eversole, D. S.; Lee, M.; Ben Yakar, A. Thermal Analysis of Gold Nanorods Heated With Femtosecond Laser Pulses. *J. Phys. D: Appl. Phys.* **2008**, *41*, 185501–185511.

47. Link, S.; Burda, C.; Mohamed, M. B.; Nikoobakht, B.; El Sayed, M. A. Femtosecond Transient-Absorption Dynamics of Colloidal Gold Nanorods: Shape Independence of the Electron-Phonon Relaxation Time. *Phys. Rev. B* **2000**, *61*, 6086–6090.

48. Berndt, P.; Fields, G. B.; Tirrell, M. Synthetic Lipidation of Peptides and Amino-Acids: Monolayer Structure and Properties. *J. Am. Chem. Soc.* **1995**, *117*, 9515–9522.